Tracking optical welding through groove modes in plasmonic nano-cavities

J. Mertens[1], A. Demetriadou[2,3], R.W. Bowman[1], F. Benz[1], M.-E. Kleemann[1], C. Tserkezis[2], Y. Shi[4], H.Y. Yang[4], O. Hess[3], J. Aizpurua[2], J.J. Baumberg[,1]*

[1] *NanoPhotonics Centre, Cavendish Laboratory, University of Cambridge, Cambridge, CB3 0HE, UK*
[2] *Centro de Física de Materiales, Centro Mixto CSIC-UPV/EHU, and Donostia International Physics Center (DIPC), Paseo Manuel Lardizabal 4, 20018 Donostia-San Sebastian, Spain*
[3] *Blackett Laboratory, Department of Physics, Imperial College London, London SW7 2AZ, United Kingdom*
[4] *Pillar of Engineering Product Development, Singapore University of Technology and Design, Singapore 138682, Singapore*

Supporting Information:

(A) Faceted 80 nm Au nanoparticles

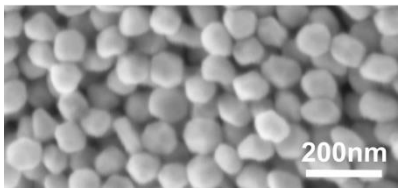

Figure S1. Scanning electron microscope image of clustered 80 nm AuNPs showing faceting.

(B) Laser irradiation of individual MoS_2 NPoMs

A power study of the irradiation of individual 80 nm MoS_2 NPoMs is performed at a wavelength of 447 nm and with laser powers of 0.6 mW, 1 mW, 1.4 mW, 2.8 mW. The laser beam is focused to a spot size of ~280 nm. The NPoM is irradiated with each laser power following the same procedure described in the main manuscript and the power is increased after 200 irradiation steps. Results of the irradiation are presented in Fig. S2a.

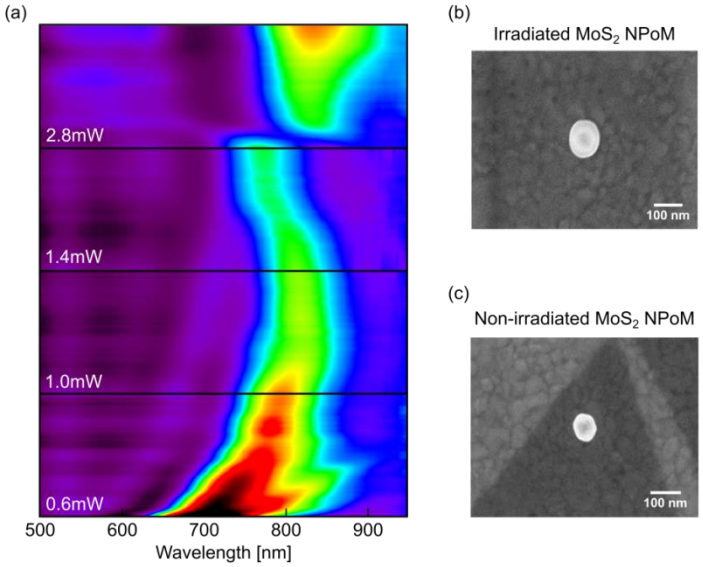

Figure S2. (a) Colour plot: scattering spectra of a MoS_2 NPoM as a function of irradiation time with different irradiation powers as indicated. Individual MoS_2 NPoM (b) which has been irradiated with a laser power of 2.8 mW and (c) which has not been irradiated.

* jjb12@cam.ac.uk

Irradiation of the MoS_2 NPoM shows red-shifts of plasmonic modes discussed in the main manuscript until the irradiation power is increased above 1.4 mW. For this power, a connection between AuNP and Au substrate is obtained, either by damaging the MoS_2 spacer or by mobilising Au atoms of the particle enough so that they can migrate through pinholes in the monolayer spacer.

An 80 nm NPoM that has been irradiated with a laser power of 2.8 mW is presented in the SEM image in Fig. S2(b). A clear increase in the size of the AuNP from 80 nm to a diameter of 100 nm is visible. A non-irradiated particle in Fig. S2c shows strong faceting. Another irradiated particle is shown in Fig. S3 from an angle of 40°, showing an elongated shape towards the underlying substrate confirming the increased facet size.

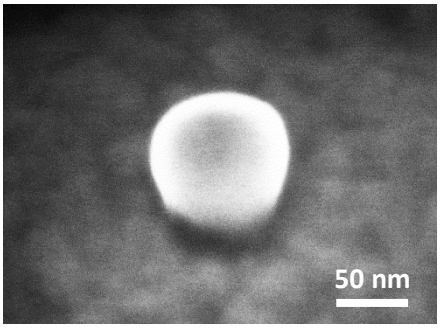

Figure S3. Electron microscope image of an irradiated nanoparticle on MoS_2. Image is recorded at an angle of 40°, showing an increased facet at the bottom of the particle.

(C) Surface enhanced Raman scattering and photoluminescence spectra of MoS_2

The surface enhance Raman scattering (SERS) spectrum and photoluminescence (PL) spectrum of an individual MoS_2 NPoM is recorded before and after illumination with 0.2 mW. No change in the spectra is observed, showing that the MoS_2 spacer is not damaged by low power laser irradiation.

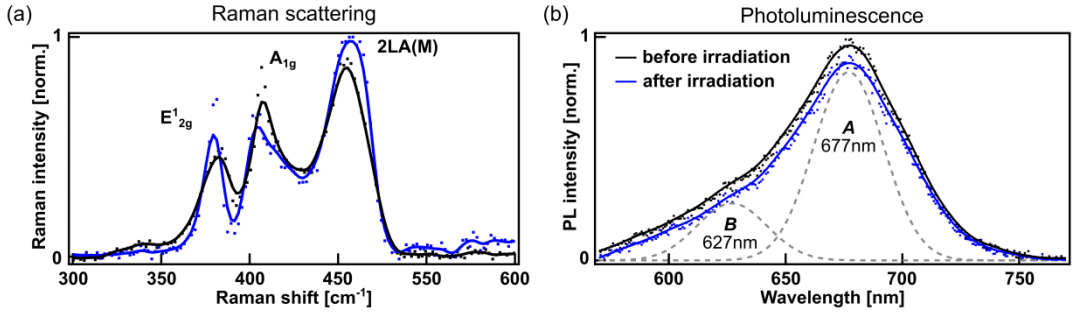

Figure S4. Comparison of the MoS_2 (a) Raman and (b) PL spectrum before (black) and after (blue) laser irradiation. Raman scattering is measured with an excitation wavelength of 633 nm; Raman modes E^1_{2g} (in-plane phonon), A_{1g} (out-of-plane phonon) and 2LA(M) (second order zone-edge phonon) are highlighted.[1] An excitation wavelength of 447 nm is used for the PL measurement. Dots are data points and solid lines are polynomial fits. Dashed grey lines in (b) are Gaussians centred at the *A*- and *B*-exciton position in MoS_2.

(D) MIM waveguide dispersion

Resonances λ_m in the groove of the conductively connected NPoM are calculated based on Eq. 2 of the main manuscript

$$\lambda_m = \frac{w-b}{m+(\varphi/2\pi)}, \qquad \text{(Eq. S1)}$$

using a fixed phase factor $\varphi = 0.4\pi$ (w: particle facet size, b: bridge width, m: mode order). The groove plasmon wavevector $k_g = 2\pi/\lambda_m$ is calculated and its energy obtained by comparison with the metal-insulator-metal planar waveguide dispersion formed of a Au-clad TPT core (Fig. S5)

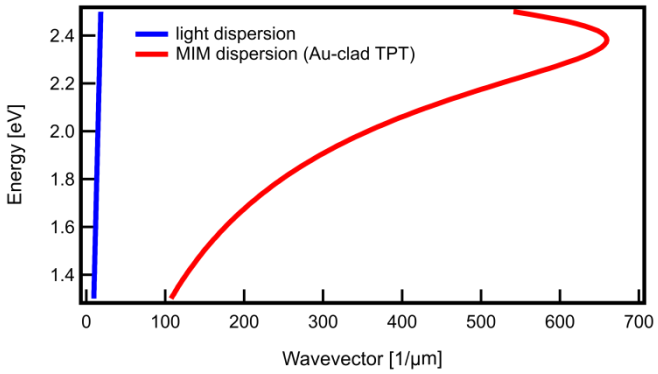

Figure S5. Dispersion relation of light in air (blue) and in the metal-insulator-metal planar waveguide (red) composed of Au cladding and 1.4 nm thick TPT core.

The MIM-dispersion relation shows the strong confinement of groove cavity modes to the gap region due to the large wavevector mismatch to the light dispersion. Therefore, transverse cavity modes do not directly radiate into the far-field and can be directly observed only in the near-field of the system. However, these cavity modes strongly couple to the plasmonic longitudinal antenna mode of the system (Fig. S6), forming new hybrid modes which have a radiative component and therefore can be detected using dark-field scattering spectroscopy. This coupling is present for both the unperturbed cavity and a conductively bridged cavity.[2,3]

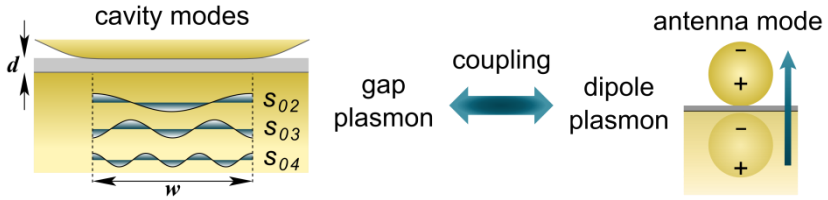

Figure S6. Schematic of the coupling between strongly confined transverse cavity modes (gap plasmon) and the radiative longitudinal antenna mode (dipole plasmon).

Previous work has shown that full electromagnetic FDTD simulations confirm this picture of coupled modes.[2] Resonance positions of the hybrid modes are calculated by solving the eigenvalues of the coupled system:

$$\overleftrightarrow{E}\boldsymbol{\psi} = \nu \cdot \boldsymbol{\psi}, \qquad \text{(Eq. S2)}$$

where $\overleftrightarrow{E}$ is a coupling matrix of order $n \times n$, $\boldsymbol{\psi}$ is the eigenvector and ν the eigenenergy of the system. The coupling matrix is composed of $n-1$ calculated groove mode energies (Eq.S1) along the diagonal elements $E_{i,i}$ (with $i = 0 \ldots n-1$) and the fixed energy position of the antenna mode $E_{n,n}$ = 1.77 eV. Off-diagonal elements $E_{i,n}$ and $E_{n,i}$ set the coupling strength between each groove mode and the antenna mode. This coupling strength is varied to obtain agreement between FDTD simulations and the MIM groove mode calculations. Eigenenergies ν of the solved eigenvalue problem provide the resonance positions of the coupled hybrid modes.

(E) Shape of AuNPs for NPoM FDTD simulations

In the theoretical simulations, the nanoparticle volume is set constant, as Au-atoms mainly migrate in the experiment towards the particle facet during laser irradiation.[4] Furthermore, we fix the particle height, since the radiative properties of our system are directly linked to the height of the nanoparticle, while the particle`s in the vicinity of the mirror strongly influences the cavity modes.[2]

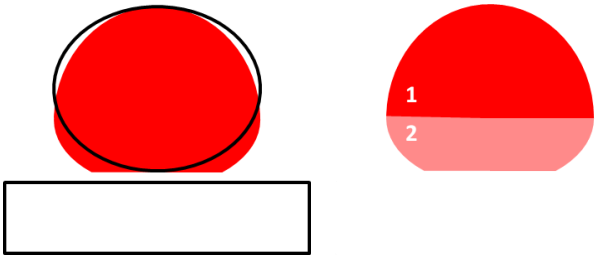

Figure S7. Schematic of the faceted NPoM geometry used in the FDTD simulations, keeping the volume and height of the nanoparticle constant for the facet growth.

Experimentally observed resonance tuning is replicated in the simulations by adjusting the nanoparticle`s morphology. Therefore, the nanoparticle is composed of two half ellipsoids (1,2 in Fig. S7), both with the same lateral radius r_{xy} but different r_z radii (i.e. r_{z1} and r_{z2}). Ellipsoid 2 is truncated to form the facet. For a given facet length, we calculate the two values for r_{z1} and r_{z2}, ensuring that the volume and height of the faceted nanoparticle remain constant.

The volume of the non-faceted nanoparticle is given by: $V_{ellips} = \frac{4}{3}\pi r_{xy}^2 (H/2)$, where H is the height of the nanoparticle. The total volume of the faceted nanoparticle is given by the volume of the top half-ellipsoid V_1 and the truncated bottom half-ellipsoid V_2:

$$V_1 = \frac{2}{3}\pi r_{xy}^2 r_{z1}, \qquad \text{(Eq. S3)}$$

$$V_2 = \frac{2}{3}\pi r_{xy}^2 \left(r_{z2} - \frac{1}{2}\frac{(r_{z2}-z_2)^2}{r_{z2}^2}(2r_{z2}+z_2) \right), \qquad \text{(Eq. S4)}$$

where z_2 is the z-value at which the second ellipsoid is truncated. This value is given by the ellipsoidal equation: $z_2 = \frac{r_{z2}}{r_{xy}}\sqrt{r_{xy}^2 - \left(\frac{w}{2}\right)^2}$, where w is the facet length. As the total height of the particle is assumed to be constant with varying facet width, the height *H* is expressed by:

$$H = r_{z1} + z_2 \Rightarrow H = r_{z1} + \frac{r_{z2}}{r_{xy}}\sqrt{r_{xy}^2 - \left(\frac{w}{2}\right)^2}. \qquad \text{(Eq. S5)}$$

As mentioned above, the volume of the deformed nanoparticle is kept constant: $V_1 + V_2 = V_{ellips}$. Solving this system of equations, the solution: $r_{z2} = 0$, $r_{z1} = H$ is obtained. This corresponds to the case where no facet is present for the nanoparticle. In contrast, re-writing the above volume conservation equation as: $V_1 - \frac{V_{ellips}}{2} = V_2 - \frac{V_{ellips}}{2} = 0$ enforces the volumes of each half-ellipsoid for the faceted nanoparticle to be equal to the half-ellipsoids' volumes of the initial particle (i.e. no facet). Hence, $V_1 = V_2$, which leads to the following relation between r_{z1} and r_{z2}:

$$r_{z1} - r_{z2} + \frac{1}{2} r_{z2} \frac{\left(r_{xy} - \sqrt{r_{xy}^2 - \left(\frac{w}{2}\right)^2}\right)^2}{r_{xy}^2} \left(2r_{xy} + \sqrt{r_{xy}^2 - \left(\frac{w}{2}\right)^2}\right) = 0. \qquad \text{(Eq. S5)}$$

Solving (Eq. S5) and (Eq. S6), leads to the following relationships for r_{z1} and r_{z2} as functions of the facet length w:

$$r_{z1} = H\left(\frac{2r_{xy}^2+\left(\frac{w}{2}\right)^2}{4r_{xy}^2+\left(\frac{w}{2}\right)^2}\right), \quad \text{(Eq. S6)}$$

$$r_{z2} = H\left(\frac{2r_{xy}^3}{\sqrt{r_{xy}^2-\left(\frac{w}{2}\right)^2}\left(4r_{xy}^2+\left(\frac{w}{2}\right)^2\right)}\right). \quad \text{(Eq. S7)}$$

At the limit of $w \to 0$, equations S6 and S7 reduce to: $r_{z1} = r_{z2} = \frac{H}{2}$, which corresponds to the non-faceted nanoparticle.

(F) Scattering and absorption cross-sections of the deformed and faceted nanoparticle

The scattering cross-section for a NPoM system with a MoS_2 ($d_{sep} = 0.6nm$, $n = 1.27$) and a TPT ($d_{sep} = 1.1$ nm, $n = 1.45$) spacer is calculated using the morphology defined in section E. Here, the non-deformed initial gold nanoparticle is obtained with $r_{xy} = 40$ nm and $H = 60$ nm.

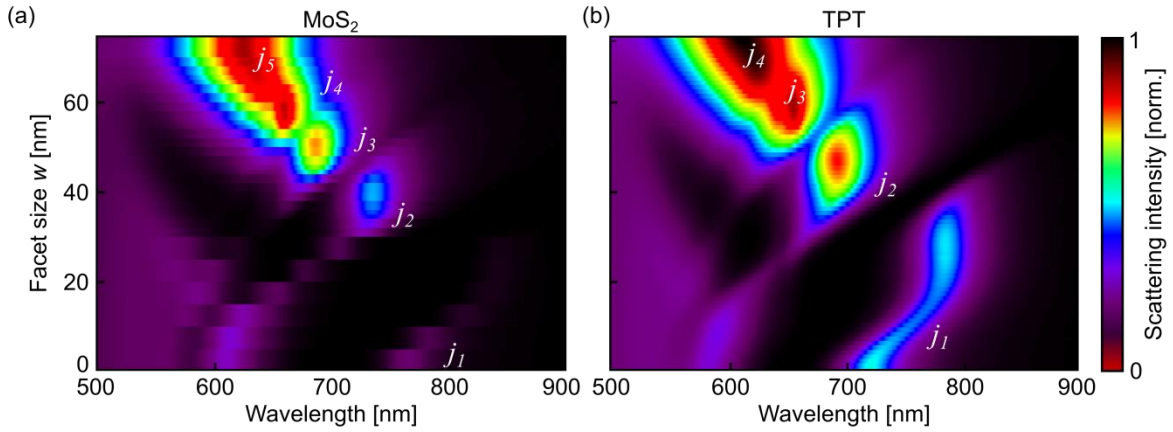

Figure S8. Colour maps of the simulated scattering spectra as a function of facet size w for (a) a MoS_2 and (b) a TPT NPoM with an 80 nm AuNP.

In the MoS_2 and TPT NPoM simulations, the nanoparticle morphology is altered in the same way in both cases (Fig. S8). The only difference in the two simulations is the thickness and optical properties of the spacer material. As observed in the figure, the two systems behave in a similar manner, in which higher-order cavity modes couple to the far-field for large facet sizes.[4,2] However, the scattering intensity for these modes varies with the facet length and is also different in the two systems studied. For the MoS_2 spacer, the j_1 (first hybrid) mode barely radiates, while j_4 and j_5 couple very strongly to the far-field. For the TPT spacer, the changes in the scattering intensity are less pronounced, with the j_1 mode radiating stronger than for MoS_2.

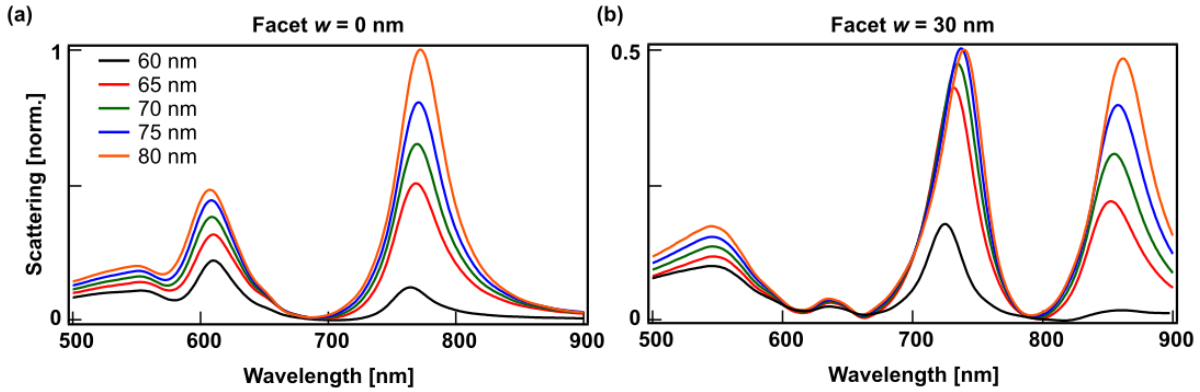

Figure S9. Simulated MoS_2 NPoM scattering spectra as a function of particle height for (a) a non-faceted and (b) a faceted $w = 30$ nm AuNP.

The height of the nanoparticle significantly impacts the radiative intensity of each excited mode. This is demonstrated by varying the AuNP height for a non-faceted particle (Fig. S9a) and for a nanoparticle with a 30 nm facet (Fig. S9b). A variation in the particle height changes the dominant radiative mode in both cases. The height of the nanoparticle mainly determines its out-coupling capabilities (antenna mode), but the radiative intensity of each mode also depends on the coupling between the transverse cavity mode and the longitudinal antenna mode. Hence, not all modes couple to the far-field with the same strength when the particle height changes and the mode resonances is not influenced because the cavity mode remains undisturbed. This difference in the scattering cross-section intensities of each mode allows determining the height of the nanoparticle present in the experiment, as small changes in the height of the nanoparticle produce large differences in the scattering cross-section.

(G) Facet growth and energy absorption under UV-illumination

The field enhancement and thus the energy distribution in the NPoM system is calculated for the UV-laser wavelength used for irradiation (450 nm). The optical field enhancement is always located at the edges of the facet facing the mirror (Fig. S10a), where a sharper facet edge produces a stronger field enhancement. The concentration of energy at the edges of the facet explains why the facet grows under UV-irradiation, with Au-atoms re-distributing themselves at the vicinity of the facet. Also, the energy can be accumulated at other sharp features of the nanoparticle (i.e. away from the mirror),[5] which eventually leads to a smoother (less faceted) nanoparticle (see SEM of Fig. S2b,c).

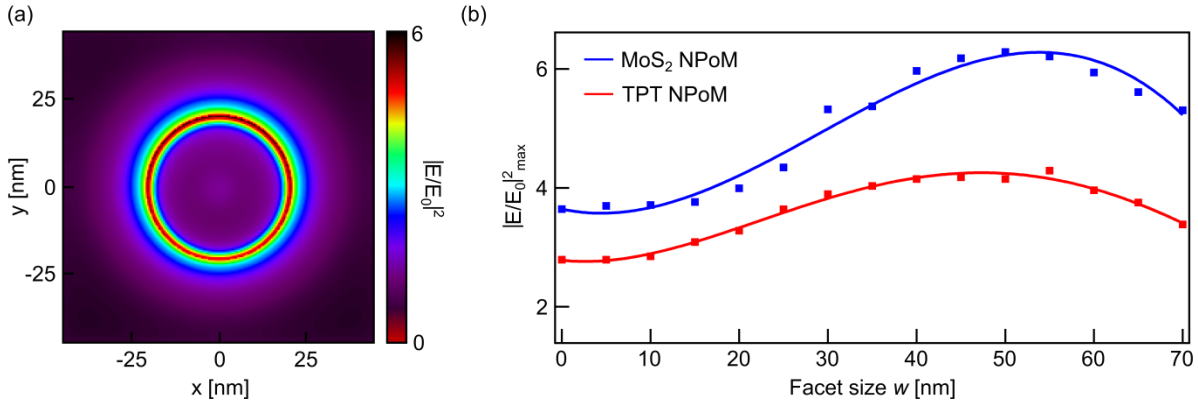

Figure S10. (a) Top-view of an 80nm MoS_2 NPoM showing the field enhancement at the facet with a diameter of w = 50 nm for a wavelength of 450 nm. (b) Maximum field enhancement of an $80\ nm$ NPoM as a function of facet size.

The field enhancement at the facet edges changes with the size of the nanoparticle's facet while the height of the particle is kept constant following the scheme presented in section E. It actually peaks at a facet size of $w \approx 50nm$ for both MoS_2 and TPT spacers, which indicates that the UV-laser can 'disturb'/move Au-atoms faster when a nanoparticle has a facet of w = 50 nm. Therefore, very rapid changes of the facet growth are expected for both TPT and MoS_2 spacers in this facet regime while a slower growth is expected for facet sizes below and above w = 50 nm.

(H) Near-field distribution of NPoMs – FDTD simulations

Near-field distributions of the bridged NPoM cavity are calculated using FDTD simulations (see methods in the main manuscript for details). A 80 nm AuNP with a w = 50 nm facet is simulated (Fig. S11). The bridge in the centre of the cavity is varied in width, increasing to a size of b = 46 nm. The far-field scattering (red) and the near-field intensity (black) are presented for each geometry in Fig. S11(a). For different resonances in the near-field indicated by dotted lines in the spectrum, the spatial near-field distribution of the electric field component perpendicular to the gap E_z is extracted as a function of the planar cavity position (Fig. S11b). A strong confinement of modes to the cavity region (light grey) is clearly observed. This distribution is strongly altered by the presence of a conductive bridge in the cavity centre (dark grey), from where the electric field is expelled resulting in two smaller groove cavities on either side of the bridge. These results support our simplified model of the bridged NPoM using a groove cavity presented in the main manuscript.

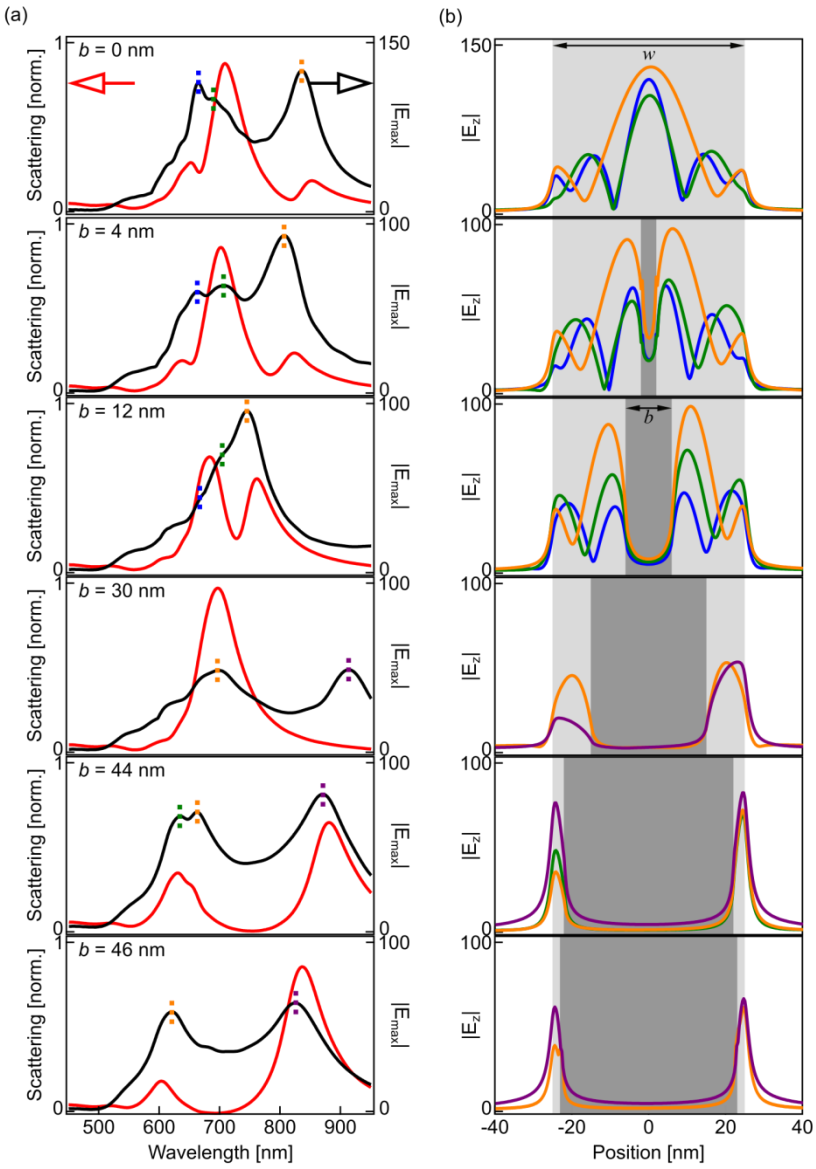

Figure S11. (a) Scattering (red) and near-field intensity (black) for a bridged 80 nm NPoM (Au-clad TPT core) with facet size w = 50 nm. The bridge size b is varied from 0 nm to 46 nm. (b) Absolute value of the z-component (along surface normal) of the electric field in the gap as a function of gap position. The near-field distribution for different energies is indicated by the colour-coded dotted lines in (a). Light grey areas show facet size (fixed), dark grey areas indicate bridge size.

(I) Bridged NPoMs for different facet sizes – FDTD simulations

Finite-difference time domain simulations are performed for TPT NPoMs with 80 nm AuNPs as a function of bridge thickness b, for different facet sizes of w = 40 nm, 50 nm, and 60 nm(Fig. S12), plotted as normalised colour maps. With increasing facet width, the number of resonances observed in the system increases. This is a result of the deeper groove cavity for which higher order resonances are allowed. Dashed grey lines k_i plotted on the simulation results are analytical solutions of the groove cavity model discussed in the main manuscript. Hybrid modes (dotted white markers) are the result of coupling between antenna mode (white dashed) and groove cavity modes. With decreasing groove cavity length, coming from the increased bridge diameter b connecting particle and surface, groove cavity resonances shift to the blue and anticross with lower order hybrid modes. Results presented in Fig. S12 show that the analytical groove cavity model fits well the simulation results of different geometries.

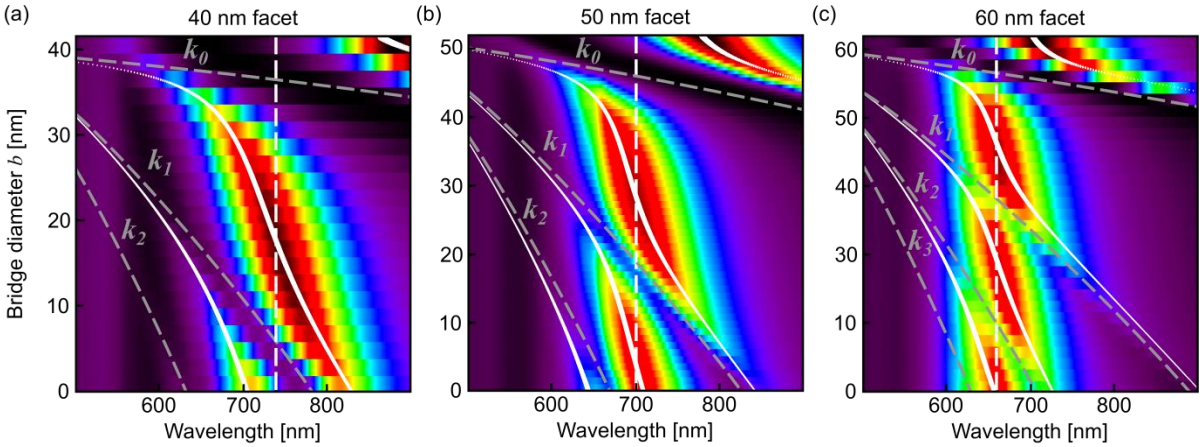

Figure S12. Finite-difference time domain simulations (normalised colour map; red: high intensity, black: low intensity) of a TPT NPoM with a facet size of (a) w = 40 nm, (b) w = 50 nm, and (c) w = 60 nm as a function of increasing conductive bridge size b linking nanoparticle and surface. Lines are analytic mode positions of cavity modes (k_i dashed grey), fixed antenna mode position (dashed white), and calculated hybrid mode positions (white lines, width gives antenna mode contribution to each hybrid mode).

(J) FDTD simulations of a NPoM with a conductive bridge at the edge of the facet

Simulation results of a TPT NPoM with a w = 50 nm facet width and a conductive bridge linking particle and surface at the edge of the particle facet are presented in Fig. S13. The plasmonic mode tuning as a function of increasing bridge diameter b is similar to the symmetric geometry with a conductive bridge in the centre of the cavity. Consistent with the results obtained for a bridge at the centre of the cavity, plasmonic modes shift to the blue and high-order groove cavity modes anticross with the antenna mode for a growing bridge at the edge. The overall tuning picture is, however, distorted in comparison to the symmetric geometry. Such distorted tuning patterns are experimentally observed as presented in Supp. Info. (H).

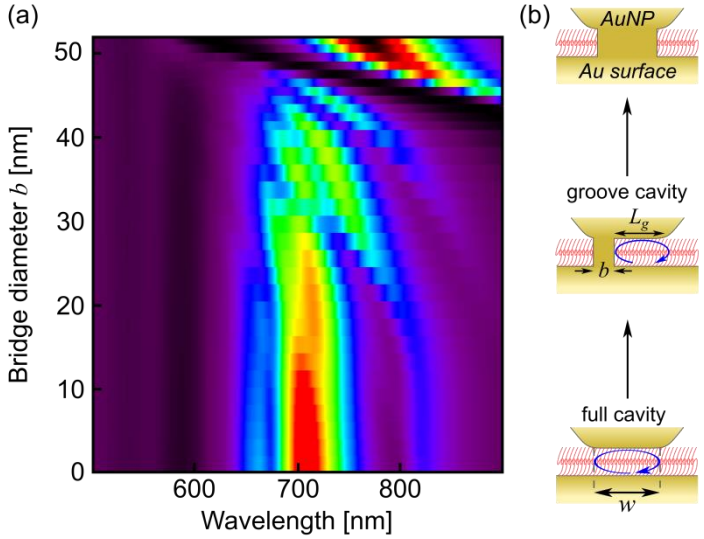

Figure S13. (a) Finite-difference time domain simulations (normalised colour map; red: high intensity, black: low intensity) of a TPT NPoM with w = 50 nm facet width and conductive bridge linking NP and surface of diameter b increased from 0 to 50 nm. The conductive bridge is pinned to the left side of the cavity and grows to the right as indicated in the schematic in (b).

(K) Simultaneous bridge and facet growth of a NPoM

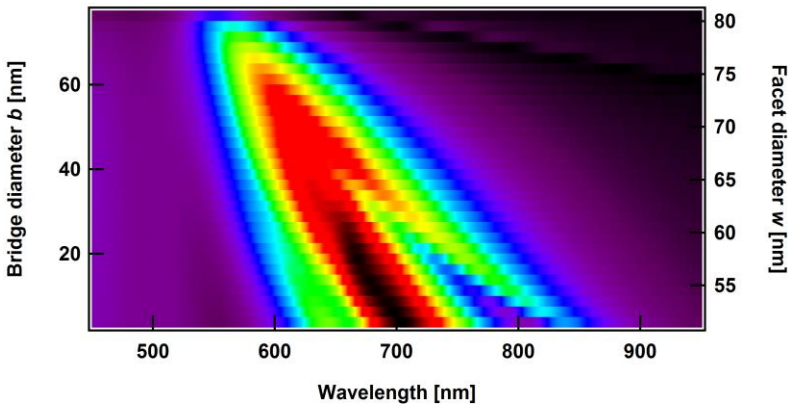

Figure S14. Finite-difference time domain simulations (normalised colour map; red: high intensity, black: low intensity) of a TPT NPoM as a function of bridge diameter b and facet width w.

In the TPT NPoM simulations discussed in the main manuscript (Fig. 3b), it is assumed that a bridge forms when the particle facet reaches a size of w = 51 nm, which then remains constant as the bridge grows. However, it is possible that the facet continues growing. Simulated scattering spectra for a TPT NPoM for which bridge and facet grow simultaneously are presented in Fig. S14. The bridge growth rate is set to be 4 times larger than the facet growth rate so that the bridge eventually fills the whole cavity.,

The FDTD simulations show different spectral shifts compared to the one discussed in the main manuscript (Fig. 3b). Mode transitions (anti-crossings) are blended, red-shift significantly and actually merge at facet size w = 67 nm and bridge size b = 48 nm. A comparison of experimental results (Fig. 3a) with simulations in Fig. S14 and Fig. 3b, leads to the conclusion that the particle facet continues to grow after a bridge is formed, but at much slower rates than at early stages of the faceting formation. In fact, the mode transitions in the experimental results resemble better the calculations where the facet stopped growing once a bridge is present (Fig. 3), revealing that in most situations facet growth slows down after the conductive bridges are formed.

(L) Irradiation of SAM NPoM – edge bridge formation

The tuning of plasmonic resonances depends strongly on the exact NPoM cavity properties. Most likely, bridge formation in the cavity due to laser irradiation does not always take place at the same position in the cavity, but is influenced by e.g. local defects in the spacer layer or the particles precise facet morphology. However, resonance tuning as a result of bridge formation always shows a similar spectral pattern as discussed in section G. For example, the experimental scattering spectra of a NPoM displayed as a function of laser irradiation time (Fig. S15) have a different tuning pattern compared to the one discussed in the main manuscript. In the manuscript it is assumed that a bridge is formed near the cavity centre. Experimental results presented in Fig. S15 resemble theoretical simulations of a bridged cavity for which the conductive link is pinned to one facet end and grows towards the cavity centre, thus filling the cavity asymmetrically from one side.

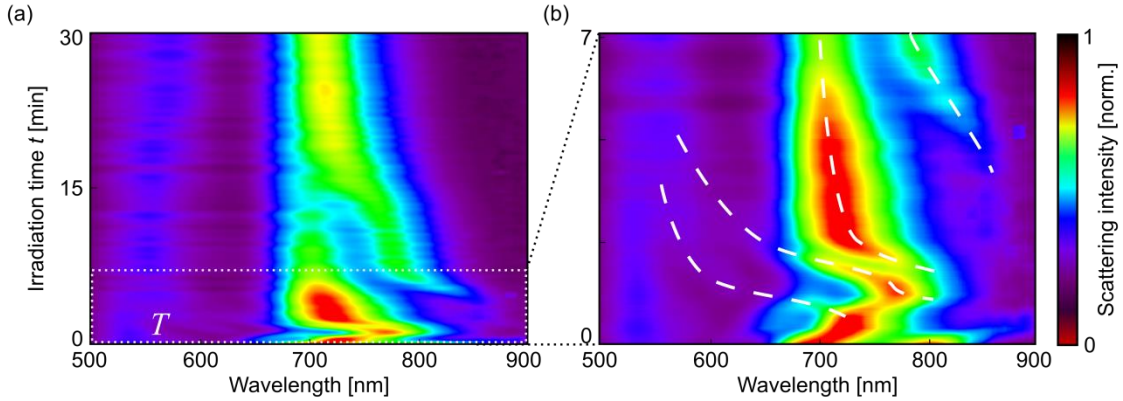

Figure S15. Colour plot of normalised dark-field NPoM scattering spectra experimentally obtained as a function of irradiation time for an individual HDT NPoM. (a) Overview of the tuning and (b) detailed presentation of the first 7 min irradiation time. Lines are a guide to the eye.

(M) Irradiation of BPDT NPoMs

Laser irradiation of NPoMs with a conductive molecular spacer does not always lead to the formation of conductive bridges across the cavity. Self-assembled monolayers of BPDT are used to separate nanoparticles from a Au surface and irradiated subsequently. Results of the irradiation are presented in the colour map of Fig. S16. Plasmonic resonances of the system only shift to the red spectral range. This shifting saturates after some irradiation time. No blue-shifts are observed in the scattering spectrum, suggesting that no conductive links are formed between particle and surface. Shunting the cavity gap using this particular conducting molecule can thus apparently reduce the forces in the NPoM system, emphasizing the versatility and specificity of the NPoM-molecular linker configuration to obtain different spectral behaviours.[6]

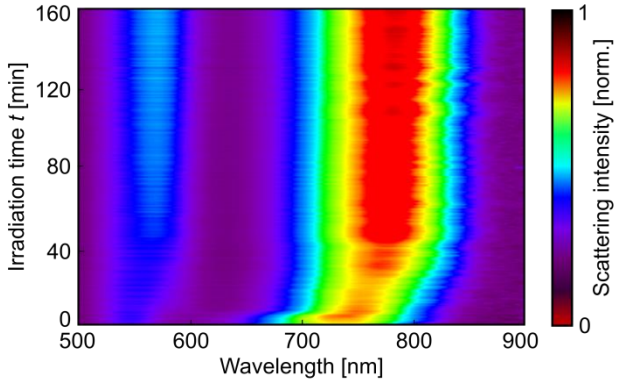

Figure S16. NPoM with BPDT spacer: experimental dark-field scattering colour map as a function of irradiation time.

(N) Formation of groove cavity

Irradiation of a NPoM on a TPT spacer leads to morphological changes of the NPoM cavity which can be described by two regimes. These regimes are, discussed in detail in the main manuscript, the non-conductive regime (Fig. S17, $t < 50$ min), in which plasmonic modes shift to the red due to a facet growth, and the conductive regime (Fig. S17, $t > 50$ min), in which multiple groove resonances are present due to the geometric and electronic bridging of the cavity. A transition from the non-conductive to the conductive regime in the experiment is very fast (see discussion on deposited energy in section G) and is not captured in the experiment. Only a sharp discontinuity is found after an irradiation time of $t = 50$ min, after which plasmonic modes shift to the red and then start blue-shifts (Fig. S17). In this transition regime (grey box Fig. S17), simulation results suggest that a groove cavity is formed via a Au protrusion, bridging the cavity and connecting AuNP with the Au surface. For the simulations, a $b = 5$ nm Au bridge is protruded in $\Delta h = 0.2$ nm steps from the AuNP until the cavity is fully bridged. A red-shift of modes is observed during this bridging process. Such bridging is likely to happen fast in the experiment and cannot be fully captured using a 1 s integration time.

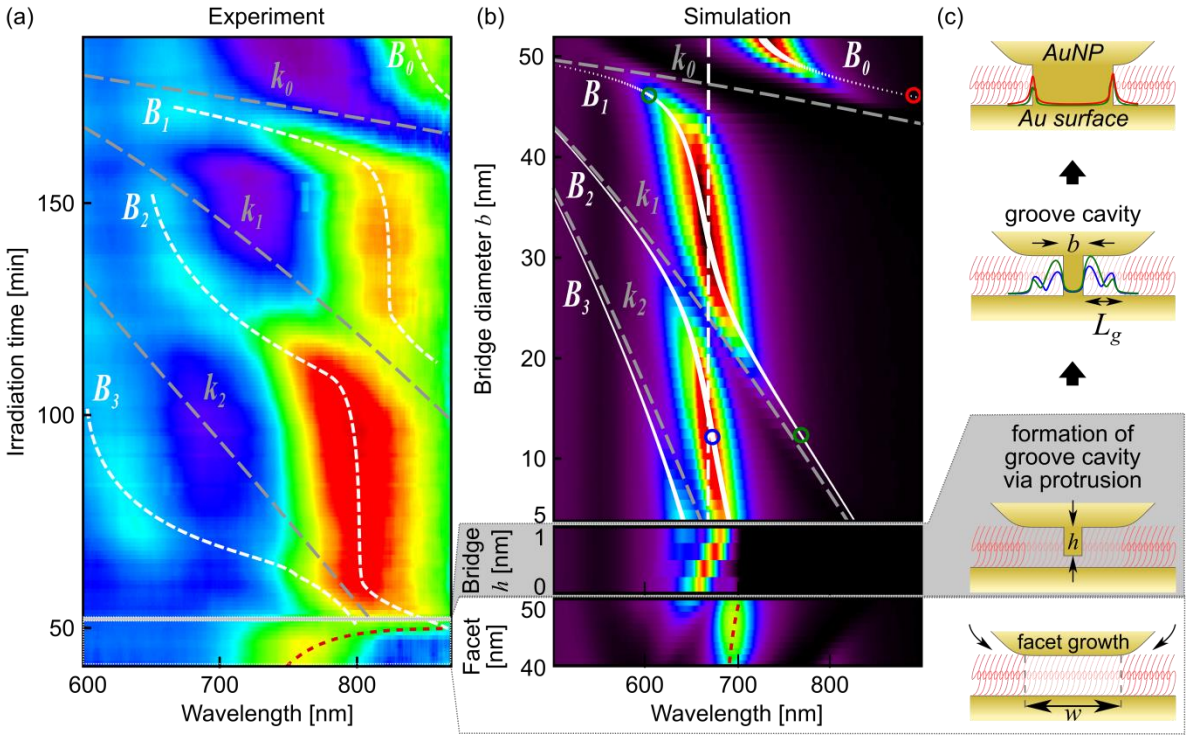

Figure S17. Modified Fig. 3 of main manuscript - Irradiation of a TPT NPoM with two regimes: Bottom panel mimics the non-conductive and top panel the conductive regime. The transition between both regimes is indicated in a grey box in (a) experimental scattering spectra, (b) FDTD simulations, and (c) schematics of the cavity model. A protrusion of a $b = 5$ nm bridge is formed bridging the gap in $\Delta h = 0.2$ nm steps, producing red-shifts of plasmonic resonances.

References:

(1) Li, H.; Zhang, Q.; Yap, C. C. R.; Tay, B. K.; Edwin, T. H. T.; Olivier, A.; Baillargeat, D. *Adv. Funct. Mater.* **2012**, *22* (7), 1385–1390.

(2) Tserkezis, C.; Esteban, R.; Sigle, D. O.; Mertens, J.; Herrmann, L. O.; Baumberg, J. J.; Aizpurua, J. *Phys. Rev. A* **2015**, *92* (5), 053811.

(3) Sigle, D. O.; Hugall, J. T.; Ithurria, S.; Dubertret, B.; Baumberg, J. J. *Phys. Rev. Lett.* **2014**, *113* (8), 087402.

(4) Sigle, D. O.; Mertens, J.; Herrmann, L. O.; Bowman, R. W.; Ithurria, S.; Dubertret, B.; Shi, Y.; Yang, H. Y.; Tserkezis, C.; Aizpurua, J.; Baumberg, J. J. *ACS Nano* **2015**, *9* (1), 825–830.

(5) Barbry, M.; Koval, P.; Marchesin, F.; Esteban, R.; Borisov, A. G.; Aizpurua, J.; Sánchez-Portal, D. *Nano Lett.* **2015**, *15* (5), 3410–3419.

(6) Benz, F.; Tserkezis, C.; Herrmann, L. O.; de Nijs, B.; Sanders, A.; Sigle, D. O.; Pukenas, L.; Evans, S. D.; Aizpurua, J.; Baumberg, J. J. *Nano Lett.* **2015**, *15* (1), 669–674.